Journal of Structural Chemistry. Vol. 56, No. 7, pp. 1253-1261, 2015.
Original Russian Text © 2015 S. A. Beyramabadi, A. Morsali, M. Pordel, H. Chegini, M. Khashi, I. Ahmadi, M. Poorzaki.

TAUTOMERIZATION OF PYRIDO[2′,1′:2,3]IMIDAZO [4,5-b]QUINOLINE-12-YLCYANIDE: A DFT STUDY

S. A. Beyramabadi, A. Morsali, M. Pordel, H. Chegini, M. Khashi, I. Ahmadi, and M. Poorzaki

UDC 541.6:547.53

The titled imidazo compound can exist as three tautomers: OH, CH, and NH forms. Firstly, the OH tautomer is produced, which can be tautomerized to the CH and NH tautomers via the intramolecular-proton transfer. Herein, employing density functional theory and handling the solvent effects with the PCM model, the structural parameters, energy behavior, and also tautomerization mechanism of the tautomers are investigated. Based on the DFT results and the obtained-AIM parameters, the CH tautomer is considered to be the most stable one. Also, the CH tautomer is a kinetically and thermodynamically controlled product in tautomerization of the OH tautomer in a methanol solution.

DOI: 10.1134/S0022476615070045

Keywords: DFT, PCM, intramolecular proton transfer, AIM analysis, tautomerization.

INTRODUCTION

Imidazo[1,2-a]pyridine derivatives are important compounds known for their useful pharmacological activities [1]. For example, gastric antisecretory [2, 3], local anesthetic [4], antiviral [5-7], hypnotic [8] and antianxiety [9] properties have been described. The nature and position of the substituent on the pyridinic moiety influence these activities [5-7]. Zolpidem is a non-benzodiazepine hypnotic of the imidazopyridine class, the leader of the international market with a blockbuster status for the treatment of sleep disorders [10].

Now, the density functional theory (DFT) as a remarkable method is widely used in many areas of the computational chemistry, such as kinetics and investigations of reaction mechanisms, spectroscopic assignments, characterization of the molecular structures, and so on [11-26].

The intramolecular proton transfer (IPT) has attracted ever increasing attention in recent years [23-26]. We have previously studied IPT in some of the chemical compounds [12-22]. Herein we theoretically describe IPT and the tautomerization of the titled compound (pyrido[2′,1′:2,3]imidazo[4,5-b]quinoline-12-yl cyanide) using the DFT approaches. Nor crystallographic structure neither theoretical study have been published for the titled compound. Therefore, an accurate and detailed theoretical investigation on this compound is of major importance.

THEORETICAL

All of the present calculations have been performed with the Gaussian 03 software package [27] using the B3LYP hybrid functional [28] and the 6-311+G(*d*,*p*) basis set.

Department of Chemistry, Mashhad Branch, Islamic Azad University, Mashhad, Iran; beiramabadi@yahoo.com, beiramabadi6285@mshdiau.ac.ir. The text was submitted by the authors in English. *Zhurnal Strukturnoi Khimii*, Vol. 56, No. 7, pp. 1318-1326, November-December, 2015. Original article submitted December 24, 2014; revised February 12, 2015.

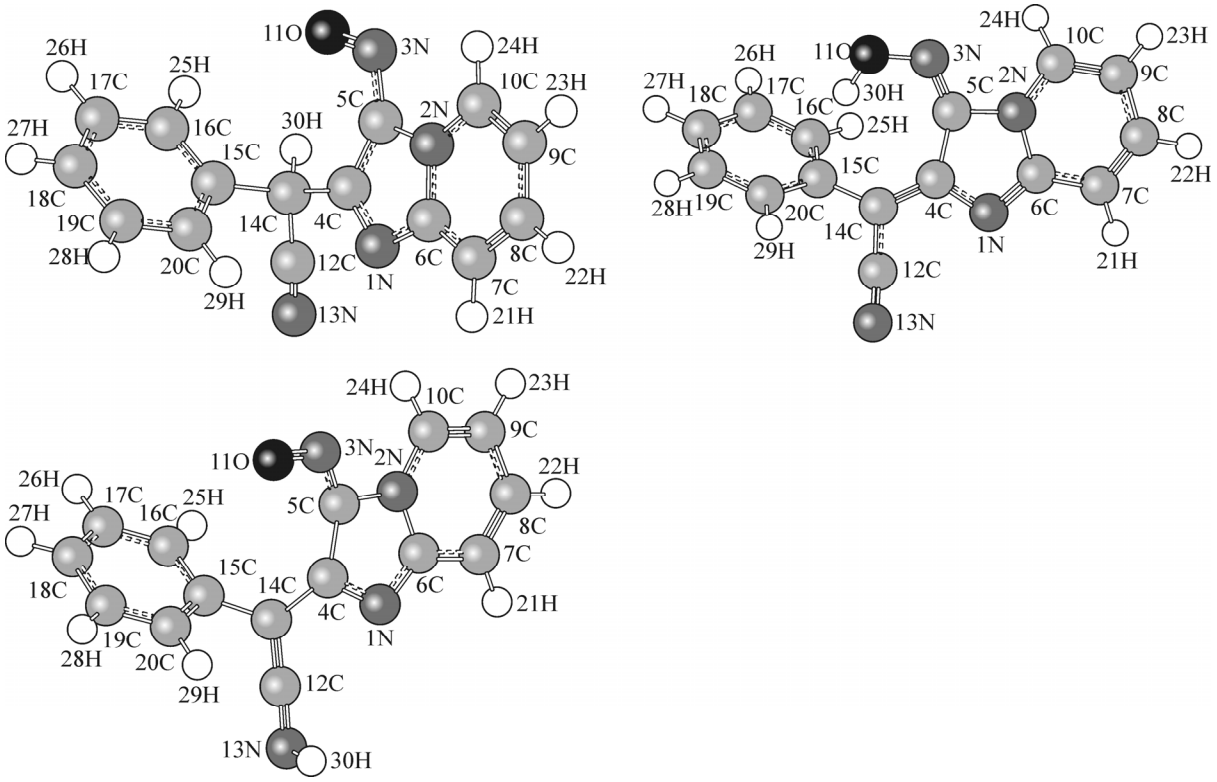

Fig. 1. Optimized geometries for the CH, OH, and NH tautomers of the titled compound.

First, all geometries were fully optimized. The optimized geometries were confirmed to have no imaginary frequency, except for transition state (TS) that has only one imaginary frequency of the Hessian. The zero-point corrections and thermal corrections have been considered in evaluation of the energies.

Here, one of self-consistent reaction field methods, the sophisticated Polarized Continuum Model (PCM) [29] has been employed for investigation of solute-solvent interactions in aqueous solution.

RESULTS AND DISCUSSION

Molecular geometry. The titled compound can exist as three possible tautomers, named as CH, OH, and NH. Their geometries have been fully optimized in the gas phase and a methanol solution using the PCM model. The experimental results show that the OH tautomer of the titled compound formed firstly [30] can be tautomerized to the CH or NH tautomers.

The PCM optimized geometries of the three tautomers are shown in Fig. 1. As seen, in the CH, OH, and NH tautomers, the H30 atom is bonded to the C14, O111, and N13 atom, respectively. IPT of the H30 atom leads to the tautomerization of the titled compounds. In continuation, its tautomerization will be investigated in details.

The relative energies of the tautomers are gathered in Table 1, where the zero-point corrections have been considered. As seen, the CH tautomer is the most stable one in both gas and solution phases.

Important structural parameters of the three tautomers are listed in Table 2. In the CH tautomer, the C14 atom is saturated with sp^3 hybridization, while it is unsaturated with the sp^2 hybridization in the OH and NH tautomers.

TABLE 1. Relative Energies ($kJ \cdot mol^{-1}$) of the CH, OH, and NH Tautomers

Species	Gas phase	PCM model
CH	0.0	0.0
OH	6.65	17.70
NH	65.80	57.44

TABLE 2. Selected Structural Parameters for the Three Tautomers of the Titled Compound and Transition States of its Tautomerism

Structural parameter	Tautomer			Transition states	
	CH	OH	NH	TS1	TS2
			Bond length, Å		
C14–H30	1.09	2.59	3.21	1.40	2.93
O111–H30	2.45	0.98	5.75	1.25	1.45
N13–H30	3.12	5.01	1.02	3.46	1.13
C14–C15	1.54	1.48	1.49	1.51	1.47
C14–C12	1.47	1.42	1.33	1.44	1.36
C12–N13	1.15	1.16	1.21	1.16	1.19
C14–C4	1.51	1.39	1.46	1.45	1.43
C4–C5	1.42	1.50	1.43	1.44	1.47
C4–N1	1.33	1.37	1.34	1.34	1.35
C5–N3	1.35	1.28	1.35	1.32	1.33
N3–O111	1.25	1.36	1.25	1.30	1.28
C5–N2	1.41	1.43	1.41	1.41	1.42
N2–C10	1.36	1.37	1.36	1.36	1.36
			Angle, deg		
C4–C14–C15	111.9	127.1	124.0	119.0	127.0
C14–C12–N13	177.9	177.8	174.8	176.6	165.5
H30–C12–N13	148.4	160.3	119.8	146.4	104.4
C4–C5–N3	136.2	116.0	137.6	126.9	141.8
C5–N3–O111	116.9	139.7	117.9	114.1	122.8
N3–O111–H30	103.7	111.8	96.2	106.4	118.4
N3–C5–N2	119.4	116.1	117.5	121.9	114.6
C5–N2–C10	130.6	128.8	130.4	130.7	129.5
N2–C10–C9	118.5	118.7	118.7	118.6	118.8
C8–C9–C10	120.3	119.4	120.1	119.8	119.8
C15–C16–C17	120.1	120.6	120.6	120.6	120.4
			Dihedral angle, deg		
C16–C15–C14–C12	–112.6	–131.3	–142.6	–46.3	–165.6
C15–C14–C12–N13	68.5	–20.2	79.2	88.5	170.9
C12–C14–C4–N1	–29.6	12.5	35.41	–26.8	–155.0
C12–C14–C4–C5	151.9	–165.5	–143.8	140.6	25.6
C14–C4–C5–N3	–4.9	19.4	9.6	–22.6	17.0
C4–C5–N3–O111	3.7	–9.7	–4.4	22.8	–4.0
N3–C5–N2–C10	2.6	–13.2	–7.9	28.5	–10.7
C5–N3–O111–H30	–25.1	–9.0	23.8	–21.2	–50.8
C7–C3–N1–C1	179.7	–177.3	–179.5	176.2	–178.1
C8–C7–C20–C19	–132.9	102.0	–55.5	123.6	–159.7
C9–C6–C15–C18	–66.7	21.5	41.2	–58.9	–151.2
C4–C5–N2–C6	–0.1	–6.5	–1.8	2.9	–4.4

In all of the three tautomers the benzene and imidazo[1,2-a]pyridine rings are not in the same plane, but make a dihedral angle of about 50° to each other.

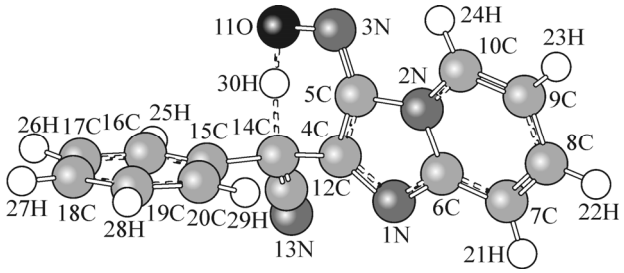

Fig. 2. The optimized geometry for the transition state of the OH⇌CH tautomerization (TS1).

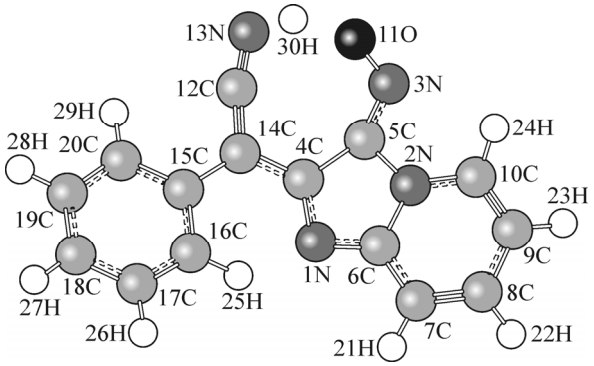

Fig. 3. The optimized geometry for the transition state of the OH⇌NH tautomerization (TS2).

Tautomerization. Our experimental results [30] show that the OH tautomer of the titled compound is formed firstly; it can be converted to the CH and NH tautomers *via* the OH⇌CH and OH⇌NH tautomerization respectively. Herein, the tautomerism of the titled compound has been investigated using the DFT approaches.

As seen from Table 1, the CH tautomer is the most stable one. In the OH⇌CH tautomerization, IPT occurs where the C14 and O11 atoms are the proton donor and acceptor respectively. The calculated D–H1…A hydrogen bond angles are 112.6° and 134.2° in the CH and OH tautomers respectively. Also, the calculated O11–N13 distances of L and L5 tautomers are 3.04 Å and 3.35 Å respectively.

Going from the OH to the CH tautomer, some of the structural parameters have changed. The C2–N3 bond length increases from 1.28 Å to 1.35 Å, whereas the N3–O11 bond length decreases from 1.36 Å to 1.25 Å. In the CH tautomer the central C14 atom has the sp^3 hybridization. The bond of the C14 atom with the C4, C12, and C15 atoms is longer than the corresponding bonds in the OH tautomer, where the C14 atom has the sp^2 hybridization. The calculated C15–C14–C12, C4–C14–C12, and C15–C14–C4 angles of CH are about 109°, which are about 120° in the OH tautomer.

In both CH and OH tautomers, the H30 and O11 atoms are on the same side of the molecule. Therefore, a low energy barrier (E_a) is predicted for the OH⇌CH tautomerization, which is 29.26 kJ·mol^{-1} and 63.62 kJ·mol^{-1} in the gas phase and the PCM model, respectively. In this reaction, the H30 atom is transferred from the C14 atom to the O11 atom. The obtained structure for the transition state of this reaction (TS1) is shown in Fig. 2. Important structural parameters of TS1 are gathered in Table 2 together with the corresponding data on the OH and CH tautomers for comparison.

In the optimized geometry of TS1, the cleavage of the C14–H30 bond together with the formation of the O11–H30 bond is clear. The C14–H30 and O11–H30 distances vary from 2.59 Å and 0.98 Å for the OH tautomer to 1.40 Å and 1.25 Å for TS1, respectively. These distances are 1.09 Å and 2.45 Å for the CH tautomer, respectively.

In the OH⇌NH tautomerization, the H30 transfers from the O11 atom to the N13 atom of the cyanide group. The optimized geometry for the transition state of this process (TS2) is shown in Fig. 3. E_a of the OH⇌NH tautomerism is predicted to be 63.29 kJ·mol^{-1} in the gas phase. With regard to the solvent effects, E_a increases to 103.53 kJ·mol^{-1} in the PCM model.

In this process, some of the structural parameters change. The N13–O11 bond length decreases from 1.36 Å (N–O single bond) to 1.25 Å (N=O double bond), whereas the C12–N13 bond length increases from 1.16 Å to 1.21 Å. The calculated D–H30…A hydrogen bond angles tautomers are 140.9° and 83.9° in OH and NH respectively. Also, the calculated O11–N13 distances of the OH and NH tautomers are 3.35 Å and 3.00 Å, respectively.

Important structural parameters of TS2 are gathered in Table 1. In the optimized geometry of TS2, the cleavage of the O11–H30 bond together with the formation of the N13–H30 bond is obvious. The O11–H30 and N13–H30 distances vary

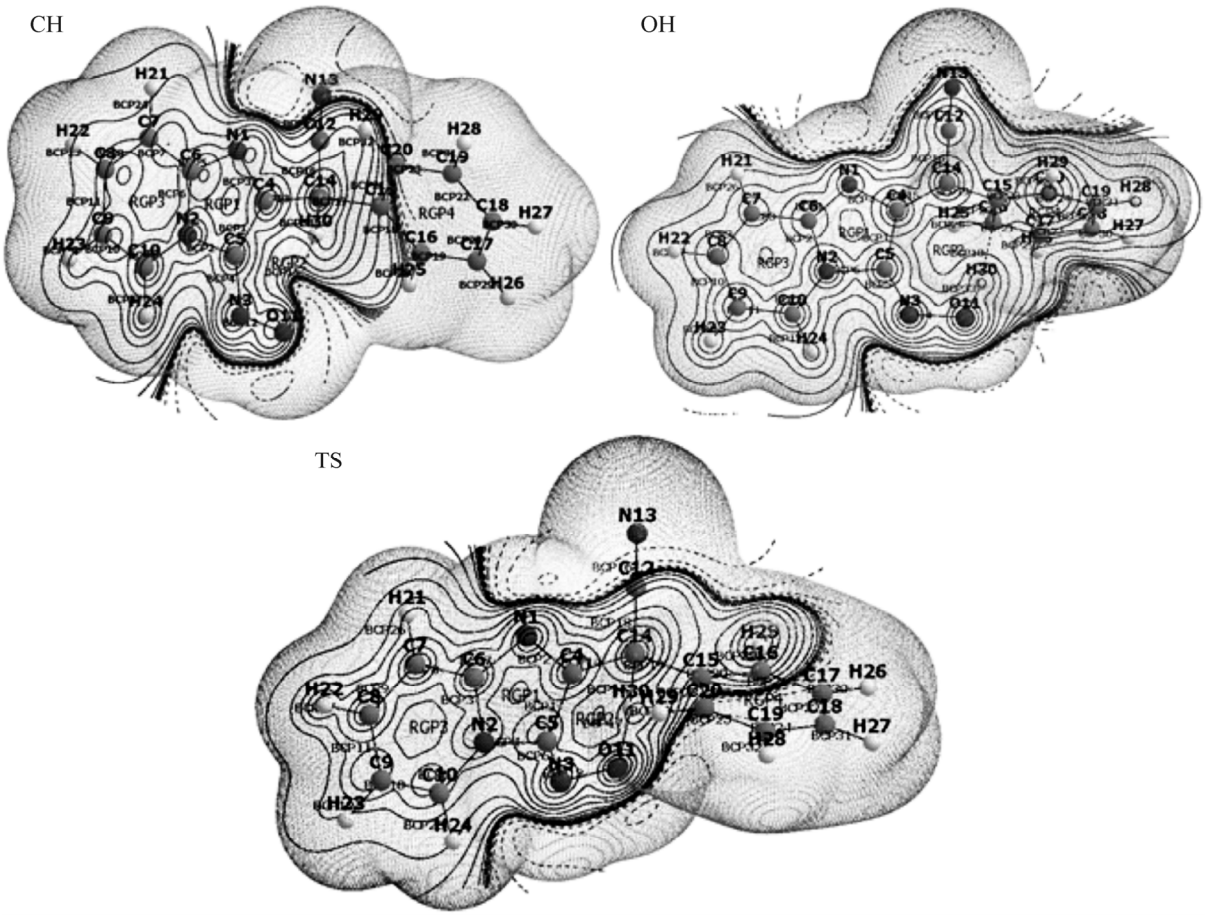

Fig. 4. Electrostatic potential map of the CH, OH, and TS1 species.

from 0.98 Å and 5.01 Å for the OH tautomer to 1.45 Å and 1.13 Å for TS2, respectively. These distances are 5.75 Å and 1.02 Å for the NH tautomer respectively.

As seen, the OH⇌CH tautomerism of the titled compound has a much lower barrier energy than the OH⇌NH tautomerism: by 34.03 kJ·mol^{-1} and 39.91 kJ·mol^{-1} in the gas phase and PCM model respectively. In addition, the CH tautomer is more stable than the NH one in the methanol solution by 57.44 kJ·mol^{-1}. Therefore, the production of the CH tautomer is kinetically and thermodynamically more favorable than that of the NH tautomer.

Electrostatic potential map. The electrostatic potential $V_S(r)$, of OH, CH**,** and TS1 is presented in Fig. 4, in which the negative potential is shown in red and the positive shown in blue. As seen in Fig. 4, there is a region of positive $V_S(r)$ in the most external part of H30 (the region located at the continuation of O111–H30) in the overall structure, but the negative potential congestion in the area of the OH structure is very prominent, indicating that IPT occurs between O111 and C14 [31-33]. Negative $V_S(r)$ is located at the outermost part of N13 from the CN substituent and an increase in the electron density concentration on C14 plays a key role in IPT given in the TS1 scheme. The interaction between the negative $V_S(r)$ region of C14 and the positive $V_S(r)$ region of H30 is one of the reasons for the intramolecular hydrogen bond formation in the molecule.

Topological analysis. The Bader theory is a very suitable tool for analyzing hydrogen bonds. The analysis and studies of the properties of bond critical points (BCPs) has often been used for the assessment of the nature of hydrogen bonds [31-33]. The parameters derived from the Bader theory, such as the electron density (ρ_{BCP}), the Laplacian of the electron density ($\nabla^2\rho$), the electron energy density H_C (the sum of the kinetic electron energy density (G_C) and the potential electron energy density (V_C)), and $-G_C/V_C$, explain the type of interaction. For a negative value of the Laplacian there is no

TABLE 3. Topological Properties at the BCPs of N…HO and NH…O Bonds in the CH, OH and TS1 Species

BCP[#]	$\|q(A\|B)\|$	$DI(A\|B)$	BPL (Bohr)	Atoms	ρ	$\nabla^2\rho$	G_C	V_C	H_C	$-G_C/V_C$
					OH					
33	0.57	0.57	1.81	O111–H30	0.35	–2.44	0.07	–0.75	–0.68	0.09
14	0.13	1.28	2.57	N3–O111	0.35	–0.54	0.21	–0.55	–0.34	0.38
5	0.64	1.46	2.43	N3–C5	0.38	–0.89	0.37	–0.95	–0.59	0.38
1	0.09	0.97	2.83	C4–C5	0.26	–0.60	0.07	–0.28	–0.22	0.24
15	0.17	1.38	2.62	C4–C14	0.31	–0.86	0.11	–0.43	–0.32	0.25
19	0.11	1.05	2.80	C14–C15	0.26	–0.63	0.07	–0.29	–0.22	0.23
20	0.07	1.31	2.66	C15–C16	0.30	–0.81	0.10	–0.39	–0.30	0.24
18	0.00	0.05	4.08	C15–H30	0.02	0.06	0.02	–0.01	0.00	1.04
					CH					
15	0.05	0.04	4.78	O111–H30	0.01	0.04	0.01	–0.01	0.00	1.15
12	0.48	1.77	2.37	N3–O111	0.46	–0.99	0.32	–0.89	–0.57	0.36
4	0.71	1.24	2.55	N3–C5	0.34	–1.05	0.21	–0.68	–0.47	0.31
1	0.10	1.15	2.69	C4–C5	0.30	–0.78	0.09	–0.38	–0.29	0.25
13	0.00	0.95	2.85	C4–C14	0.25	–0.60	0.06	–0.27	–0.21	0.22
17	0.11	0.94	2.91	C14–C15	0.24	–0.52	0.05	–0.24	–0.18	0.23
18	0.07	1.36	2.64	C15–C16	0.31	–0.85	0.10	–0.41	–0.31	0.24
33	0.07	0.86	2.04	C14–H30	0.28	–0.96	0.04	–0.31	–0.28	0.11
					TS					
17	0.33	0.38	2.36	O111–H30	0.17	–0.17	0.08	–0.21	–0.13	0.40
13	0.26	1.47	2.48	N3–O111	0.40	–0.70	0.25	–0.68	–0.43	0.37
6	0.64	1.37	2.48	N3–C5	0.36	–0.98	0.30	–0.85	–0.55	0.36
1	0.06	1.03	2.74	C4–C5	0.29	–0.74	0.08	–0.35	–0.27	0.24
14	0.24	1.08	2.76	C4–C14	0.27	–0.69	0.08	–0.33	–0.25	0.24
19	0.09	0.98	2.86	C14–C15	0.24	–0.54	0.06	–0.26	–0.20	0.24
23	0.04	1.35	2.65	C15–C20	0.31	–0.84	0.10	–0.41	–0.31	0.24
15	0.09	0.38	2.65	C14–H30	0.13	–0.16	0.04	–0.12	–0.08	0.33

[#] The number of BCP as in Fig. 4.

doubt that the interaction or bond formation is covalent. If $\nabla^2\rho$ and H_C are positive, the interaction is non-covalent. If $\nabla^2\rho$ is positive but H_C is negative, and $-G_C/V_C$ is smaller than 1, then the interaction can be classified as partly covalent in nature [34-37].

The topological parameters, such as ρ_{BCP}, $\nabla^2\rho$, G_C, V_C, and H_C at the BCPs of C…HO, CH…O, and C…H…O bonds are listed in Table 3. Also, the molecular graphs are shown in Fig. 4. The molecular graphs show that there is a BCP between the H30 and C14 atoms, which are linked by two bond paths. The topological structure indicates that the H30 atom of the OH tautomer could transfer to the C14 atom. Table 3 shows that at the BCP of the hydrogen bond, both $\nabla^2\rho$ and H_C are positive, indicating that the intramolecular proton interaction is noncovalant; all of the topological parameters show that the intramolecular hydrogen bond is partly covalent in nature [38]. All values given in Table 3 have convinced us that the IPT process certainly occurs. Considering the values of ρ_{BCP} and the bond path between H30–C14, we reveal that the location of the H30 atom on the C14 is more stable than that on the O11 atom. Thus, it seems that the proton transfer occurs through a high energy barrier.

Delocalization index (*DI*(O,H), *DI*(C,H)). Based on the *DI* definition in the study of Fradera et al. [39, 40], *DI* is the number of electron pairs shared by two basins, although their definition cannot be a proof for the idea that *DI* is the function of a bond order. Ánglyán et al. [41] have found that it can explain the covalent bond order [42].

TABLE 4. Topological Properties at the RCP, the Distance between RCP and BCP (ρ_{RCP} in atomic units and $d_{RCP\rightarrow BCP}$ in nm)

Atoms	ρ	$\nabla^2\rho$	K	BCP–RCP	$d_{RCP\rightarrow BCP}$ (Bohr)
		OH			
–N3–C5–C4–C14–C15–H30–O111–	0.00864	0.04123	–0.00195	BCP18–RCP2	1.876
				BCP33–RCP2	2.239
				BCP14–RCP2	3.064
				BCP5–RCP2	2.945
				BCP1–RCP2	2.692
				BCP15–RCP2	2.837
				BCP19–RCP2	2.946
		CH			
–N3–C5–C4–C14–H30–O111–	0.00992	0.04765	–0.00199	BCP15–RCP2	1.047
				BCP12–RCP2	2.870
				BCP4–RCP2	2.867
				BCP1–RCP2	2.685
				BCP13–RCP2	2.673
				BCP33–RCP2	2.464
		TS			
–N3–C5–C4–C14–H30–O111–	0.02387	0.15145	–0.0057	BCP15–RCP2	1.851
				BCP17–RCP2	1.702
				BCP13–RCP2	2.291
				BCP6–RCP2	2.228
				BCP1–RCP2	2.169
				BCP14–RCP2	2.489

*DI*s of the intramolecular C…H and O…H hydrogen bonds formed are listed in Table 3. With this information in hand, it can be seen that all *DI* values were small implying that the covalent interactions between O–H and C–H were weak.

The withdrawing cyanide substitution on the C14 atom leads to a decrease in the *DI* value, so the non-covalent bonding becomes weaker and the charge contribution to the bond between A and B atoms (q(A|B)) confirms this idea; the values of charge transfer along the bond path have a direct relation to *DI* that can explain the bond strength. The withdrawing effect of the cyanide group increases the attractive force of the C14 atom on the H30 proton. This is confirmed by the transferred charge between the C14 and H30 atoms together with the elongation of the C14–H30 bond with respect to the O111–H30 form.

AIM analysis on RCP. RCP is a point of the minimum electron density within the ring surface and a maximum on the ring line [43]. Table 4 gives the information about the electron density ρ_{RCP} at the RCP and $\nabla^2\rho_{RCP}$ of the ring (H–O–N–C–C–C), produced by the hydrogen bond formation. The distances between the RCP, the BCP of the hydrogen bond, and the BCP in the ring bond path are listed in Table 4. It is known that –CN being a strong electron withdrawing group increases the bond strength, meaning that ρ_{RCP}, $\nabla^2\rho_{RCP}$ and K (the Hamiltonian form of the kinetic energy density) increased, so the C14–H30 form is more stable than the O111–H30 form. In other words, the CH tautomer is more stable than the OH one [31, 32]. Along with this effect the RCP–BCP distance decreases the bond strength. These observations are compatible with Bader's AIM theory.

When the proton transfer occurs, $d_{RCP\rightarrow BCP}$ of O…H and C…H changes to 1.876 Bohr and 1.046 Bohr, respectively. This change in $d_{RCP\rightarrow BCP}$ has a noticeable value. The largest amount of ρ_{RCP}, $\nabla^2\rho_{RCP}$ and the lowest of $d_{RCP\rightarrow BCP}$ are the indication of the highest hydrogen bond strength. It means that the RCP properties, such as ρ_{RCP}, $\nabla^2\rho_{RCP}$ and $d_{RCP\rightarrow BCP}$, can be properly used to predict the behavior and strength of the intramolecular hydrogen bond. The K values confirm this matter, too.

CONCLUSIONS

Based on the experimental results, the OH tautomer of the titled compound is formed firstly. This tautomer can be tautomerized to the CH and NH forms via the OH⇌CH and OH⇌NH tautomerization, respectively. In this work, the tautomerism of the titled compound has been investigated in details using the DFT approaches. The PCM model was used to explore the effects of methanol solvent molecules.

Based on the DFT results, it can be concluded that the CH tautomer is the most stable one in both gas phase and aqueous solution. In addition, E_a of the OH⇌CH tautomerism is 34.03 kJ·mol^{-1} and 39.91 kJ·mol^{-1} being lower than E_a of the OH⇌NH tautomerism in the gas phase and the PCM model, respectively. Since, the CH tautomer is a kinetically and thermodynamically controlled product in the tautomerization of the OH tautomer in a methanol solution.

The obtained AIM parameters play an essential role in the identification of the most stable tautomer. These parameters demonstrate that the CH tautomer is the most stable tautomer of the titled compound.

We gratefully acknowledge financial support from the Islamic Azad University, Mashhad Branch.

REFERENCES

1. H.-J. Knölker, R. Boese, and R. Hitzemann, *Chem. Ber*., 123, 327-329 (1990) and references therein.
2. J. J. Kaminski, J. A. Bristol, C. Puchalski, R. G. Lovey, A. J. Elliott, H. Guzik, D. M. Solomon, D. J. Conn, M. S. Domalski, S. C. Wong, E. H. Gold, J. F. Long, J. S. Chiu, M. Steinberg, and A. T. McPhail, *J. Med. Chem*., **28,** 876-892 (1985).
3. J. J. Kaminski and A. M. Doweyko, *J. Med. Chem*., **40,** 427-436 (1997).
4. P. Sanfillipo, M. Urbanski, J. B. Press, B. Dubinsky, and J. B. Moore, *J. Med. Chem*., **31,** 2221-2227 (1988).
5. A. Gueiffier, M. Lhassani, A. Elhakmaoui, R. Snoeck, G. Andrei, O. Chavignon, J. C. Teulade, A. Kerbal, E. M. Essassi, J. C. Debouzy, M. Witvrouw, Y. Blache, J. Balzarini, E. De Clercq, and J. P. Chapat, *J. Med. Chem*., **39,** 2856-2859 (1996).
6. A. Gueiffier, S. Mavel, M. Lhassani, A. Elhakmaoui, R. Snoeck, G. Andrei, O. Chavignon, J. C. Teulade, M. Witvrouw, J. Balzarini, E. De Clercq, and J. P. Chapat, *J. Med. Chem*., **41,** 5108-5112 (1998).
7. M. Lhassani, O. Chavignon, J. M. Chezal, J. C. Teulade, J. P. Chapat, R. Snoeck, G. Andrei, J. Balzarini, E. De Clercq, and A. Gueiffier, *Eur. J. Med. Chem*., **34,** 271-274 (1999).
8. J. P. Kaplan and P. George, *Chem. Abstr*., **97,** 149531a (1982).
9. P. George, G. Rossey, M. Sevrin, S. Arbilla, H. Depoortere, and A. E. Wick, in: *Imidazopyridines in Anxiety Disorders: A Novel Experimental and Therapeutic Approach*, G. Bartholini, M. Garreau, P. L. Morselli, and B. Zivkovic (eds.), Raven Press, New York (1993), pp. 49-59.
10. J. D. Hoehns and P. J. Perry, *Clin. Pharmacol*., **12,** 814-828 (1993).
11. B. Edwin and I. H. Joe, *J. Mol. Struct*., **1034,** 119-127 (2013).
12. H. Eshtiagh-Hosseini, M. R. Housaindokht, S. A. Beyramabadi, S. Beheshti, A. A. Esmaeili, M. Javan-Khoshkholgh, A. Morsali, *Spectrochim. Acta, Part A*, **71,** 1341-1347 (2008).
13. S. A. Beyramabadi, A. Morsali, M. Javan-Khoshkholgh, and A. A. Esmaeili, *Spectrochim. Acta, Part A*, **83,** 467-471 (2011).
14. Z. Sadeghzade, S. A. Beyramabadi, and A. Morsali, *Spectrochim. Acta, Part A*, **138,** 637-642 (2015).
15. S. A. Beyramabadi, A. Morsali, S. H. Vahidi, M. Javan Khoshkholgh, and A. A. Esmaeili, *J. Struct. Chem*., **53,** 665-675 (2012).
16. H. Eshtiagh-Hosseini, S. A. Beyramabad, A. Morsali, M. Mirzaei, H. Chegini, M. Elahi, and M. A. Naseri, *J. Mol. Struct*., **1072,** 187-194 (2014).

17. S. H. Vahidi, A. Morsali, and S. A. Beyramabadi, *Comput. Theor. Chem*., **994,** 41-46 (2012).
18. S. A. Beyramabadi, H. Eshtiagh-Hosseini, M. R. Housaindokht, and A. Morsali, *Organometallics*, **27,** 72-78 (2008).
19. S. A. Beyramabadi, H. Eshtiagh-Hosseini, M. R. Housaindokht, and A. Morsali, *J. Mol. Struct.: THEOCHEM*, **903,** 108-114 (2009).
20. H. Eshtiagh-Hosseini, S. A. Beyramabadi, M. R. Housaindokht, and A. Morsali, *J. Mol. Struct.: THEOCHEM*, **941,** 138-143 (2010).
21. H. Eshtiagh-Hosseini, M. R. Housaindokht, S. A. Beyramabadi, S. H. Mir Tabatabaei, A. A. Esmaeili, and M. Javan-Khoshkholgh, *Spectrochim. Acta, Part A*, **78,** 1046-1050 (2011).
22. S. A. Beyramabadi, A. Morsali, M. Javan-Khoshkholgh, and A. A. Esmaeili, *J. Struct. Chem*., **53,** 460-467 (2012).
23. Y. L. Lin and J. Gao, *Biochemistry*, **49,** 84-94 (2010).
24. W. Rodríguez-Córdoba, J. S. Zugazagoitia, E. Collado-Fregoso, and J. Peon, *J. Phys. Chem. A*, **111,** 6241-6247 (2007).
25. M. Sauer, C. Yeung, J. H. Chong, B. O. Patrick, and M. J. MacLachlan, *J. Org. Chem.*, **71,** 775-788 (2006).
26. A. Jezierska-Mazzarello, R. Vuilleumier, J. J. Panek, and G. Ciccotti, *J. Phys. Chem. B*, **114,** 242-253 (2010).
27. M. J. Frisch et al., *Gaussian 03, Revision B.03*, Gaussian Inc., Pittsburgh, PA (2003).
28. C. Lee, W. Yang, and R. G. Parr, *Phys. Rev. B*, **37,** 785-789(1988).
29. R. Cammi and J. Tomasi, *J. Comput. Chem*., **16,** 1449-1458 (1995).
30. M. Pordel, S. A. Beyramabadi, and A. Mohammadinejad, *Dyes Pigm*., **102,** 46-52 (2014).
31. X. Li, Y. Wang, S. Zheng, and L. Meng, *Struct. Chem*., **23,** 1233-1240 (2012).
32. H. Eshtiagh-Hosseini, S. A. Beyramabadi, A. Morsali, M. Mirzaei, H. Chegini, M. Elahi, and M. A. Naseri, *J. Mol. Struct*., **1072,** 187-194 (2014).
33. P. Gilli, V. Bertolasi, V. Ferretti, and G. Gilli, *J. Am. Chem. Soc*., **116,** 909-915 (1994).
34. S. Jenkins and I. Morrison, *Chem. Phys. Lett*., **317,** 97-102 (2000).
35. R. F. Bader, *Atoms in Molecules: A Quantum Theory*, Oxford University Press, Oxford (1990).
36. C. F. Matta, A. A. Arabi, and D. F. Weaver, *Eur. J. Med. Chem*., **45,** 1868-1872 (2010).
37. S. J. Grabowski and M. Malecka, *J. Phys. Chem. A*, **110,** 11847-11854 (2006).
38. R. N. Musin and Y. H. Mariam, *J. Phys. Org. Chem*., **19,** 425-444 (2006).
39. X. Fradera, M. A. Austen, and R. F. Bader, *J. Phys. Chem. A*, **103,** 304-314 (1999).
40. J. Poater, M. Sola, M. Duran, and X. Fradera, *Theor. Chem. Acc*., **107,** 362-371 (2002).
41. J. G. Angyan, M. Loos, and I. Mayer, *J. Phys. Chem*., **98,** 5244-5248 (1994).
42. Y. Mo and S. D. Peyerimhoff, *J. Chem. Phys*., **109,** 1687-1697 (1998).
43. R. F. Bader, M. T. Carroll, J. R. Cheeseman, and C. Chang, *J. Am. Chem. Soc*., **109,** 7968-7979 (1987).